

Doping-dependent studies of the Anderson-Mott localization in polyaniline at the metal-insulator boundary

G. Tzamalís,¹ N. A. Zaidi,¹ C. C. Homes,² and A. P. Monkman¹¹*Department of Physics, University of Durham, South Road, Durham DH1 3LE, United Kingdom*²*Department of Physics, Brookhaven National Laboratory, Upton, New York 11973-5000*

(Received 19 February 2002; published 5 August 2002)

Temperature-dependent dc conductivity measurements and infrared reflectivity measurements (20–9000 cm^{-1}) were performed on a series of polyaniline samples with two different dopant acids at various doping levels. The typical fingerprints of a disordered metal such as a positive temperature coefficient of resistivity at high temperatures, a very high reflectivity in the far infrared, and a plasma resonance have been observed. The results were analyzed in the framework of the Anderson-Mott localization model and considerable consistency between transport studies and optical measurements was obtained. Various parameters enabling a comparative classification of the materials are also reported.

DOI: 10.1103/PhysRevB.66.085202

PACS number(s): 78.20.Ci

I. INTRODUCTION

Before the discovery of metallic poly(sulfur nitride) $(\text{SN})_x$ and the enhancement of conductivity in doped Shirakawa polyacetylene on the order of 10^3 S/cm, the polymeric materials were considered as insulators. During the past fifteen years, a significant improvement in methods of processibility of polyconjugated systems has led to a reduction in the structural and morphological disorder, bringing forth a new generation of conductive polymers with considerably high values of conductivity and excellent environmental stability. In particular, conductivities on the order of 10^4 S/cm were observed at 1987 in iodine-doped Naarman $(\text{CH})_x$ and further studies¹ have reported conductivity values higher by one order of magnitude, which is comparable to those of traditional metals. Although the majority of conjugated polymers do not show such high conductivity values, their study can provide an understanding of the physical properties for this class of materials.

A common feature of all conductive polymers is the fact that they are insulators in their pure (pristine) form, and only after doping (protonation) they become conductive. The increase in conductivity induced by doping can be of ten orders of magnitude or more, indicating the suitability of conjugated polymers for a systematic study of the metal-insulator transition. The key role held by the doping in the metal-insulator transition has been widely and unequivocally acknowledged in the field.^{2–4} Nevertheless, its effect on the nature of the metallic states is still debated as many different models have been proposed.

The doping process in conducting polymers is entirely different from that in semiconductors since the dopants are not substitutional, but interstitial. The dopants are inserted between the chains rather than replacing host atoms, and, dependent on the redox process, can either oxidize to create a positive charge or reduce and create a negative charge on the chain. The charge carriers generated by doping, due to the quasi-one-dimensional nature of polymer chains, are stored in nonlinear excitation states such as solitons, polarons, and bipolarons.⁵ Whether these excitations can be

have as free carriers or not is determined by the interchain interaction, the carrier density, and the extent of disorder.

Disorder along with interchain interaction and doping level determine the insulator-metal (*I-M*) transition in conducting polymers. The relative importance and precise contribution of those factors in the nature of *I-M* transition remains controversial. Nevertheless, the metallic behavior exhibited by some polymers implies that there is a continuous density of states near the Fermi energy, whose extent, characterized by the localization length L_C , decreases as disorder increases.

The extent of the disorder and a consequent characterization of the transport behavior of a material is usually quantified using some criteria, mostly derived from the existent theory on *I-M* transitions^{6,7} and have been applied for various materials.^{2,3} The principal criterion for the existence of a metallic state is a finite dc conductivity at $T \rightarrow 0$ K that confirms the presence of delocalized states at the Fermi level. Where mK measurements are not feasible, the metallic behavior, in the case of disordered metallic systems with a weakly negative temperature coefficient of resistivity (TCR), can be identified by a positive temperature coefficient of the reduced activation energy plot $W = d(\ln \sigma)/d(\ln T)$.⁸ Additional fingerprints of the metallic state such as the very high infrared reflectivity and a Drude-like behavior of the dielectric function of the material can be inferred from infrared reflectivity measurements. Optical measurements can provide information about the charge carrier dynamics over a wide energy range, through processes occurring on smaller time scales ($\sim \omega^{-1}$) than transport ones, and, with the application of an appropriate model, could give further evidence about the extent of the disorder and other significant parameters for the understanding of the *I-M* transition.

In this paper, further transport and optical measurements on polyaniline (PANi) films doped with two different acids and at various doping levels are reported. The dopants used on the emeraldine base (EB) form of PANi were 2-acrylamido-2-methyl-1-propanesulfonic acid (AMPSA) and 10-camphorsulfonic acid (CSA). The different doping levels that characterize each film purport to clarify, within

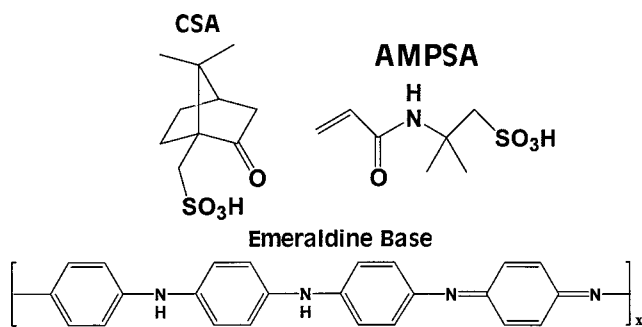


FIG. 1. Structures for the emeraldine base (EB) form of polyaniline, 2-acrylamido-2-methyl-1-propanesulphonic (AMPSA), and 10-camphorsulphonic acid (CSA).

the context of the localization modified Drude model,⁶ the effect of the doping level on the metallic state, if any, of this material. The characteristics of each sample will be quantitatively reported expanding previous studies on PANi-AMPSA samples,⁹ in order to provide a comprehensive classification of the doped-polyaniline systems.

II. EXPERIMENTAL PROCEDURE

A. Sample preparation

The emeraldine base form of PANi with high molecular weight ($M_w \sim 2 \times 10^5 \text{ g mol}^{-1}$), synthesized in Durham at 248 K,^{10,11} was used as our starting material. Two categories of PANi free standing films were obtained in the following way: EB and the doping acid (either CSA or AMPSA) were mixed in an agate mortar and pestle at various molar ratios and added to the appropriate solvent (*m*-cresol for PANi-CSA and dichloroacetic acid for PANi-AMPSA sample) to obtain a 2% w/w solution concentration. The solution was homogenized until complete dissolution, poured onto silicon wafers, and left to dry in an oven at 353 K for 24 h. The free standing films (emeraldine salts) were peeled from the silicon wafers and labeled according to the molar ratio of the dopant to the EB. For instance, a 50% doping level means that all the imine nitrogens in a four ring EB repeat unit (half-oxidized form) are protonated. The thicknesses of the films ranged from 30–100 μm and they were considered isotropic since this method of preparation does not favor any particular anisotropy. Factors such as the solution concentration, the solvent evaporation rate, and other random elements incurred through the preparation procedure, have an effect on the degree of the disorder present on the sample,^{12,13} however, a variety of measurements performed on samples with the same characteristics has demonstrated a considerable repeatability that makes it feasible to discuss of certain distinctive physical tendencies in the samples. The structures for the EB form of PANi along with CSA and AMPSA are shown in Fig. 1.

B. Temperature-dependent dc conductivity measurements

Temperature-dependent conductivity measurements were performed inside a closed-loop helium cryostat under dynamic vacuum ($\sim 10^{-4}$ mbar). The temperature range was

10–295 K. Four gold strips were evaporated on the sample surface to provide the best possible contacts between the four in-line electrodes formed on a printed circuit board, and the sample. The sample was afterwards securely mounted on the cryostat's cold finger in a way that the pressure exerted on the sample surface was constant and homogeneous. The whole configuration aims to minimize the contact resistance between the sample and the electrodes so that the conductivity values are as accurate as possible.

Before data acquisition, the linear response of the samples as defined by the current-voltage curves was confirmed. For each voltage measurement, the applied current was 1 mA so that the dissipated power into the sample did not exceed 1 μW . The measurements were made when a constant temperature throughout had been achieved, ensuring that the sample was in thermal equilibrium with its surroundings. At each temperature, 100 voltage measurements were taken and averaged for increased precision. Finally, the conductivity values were obtained using Ohm's law after having accurately measured the dimensions of the sample.

C. Infrared reflectivity measurements

Normal incidence infrared measurements between 20 and 9000 cm^{-1} (or 0.002–1.116 eV) were taken using a Bruker IFS66v/S Fourier transform interferometer at NSLS (Beamline U10A) in Brookhaven National Laboratory.⁹ Each sample was visually inspected for surface quality sufficient to minimize scattering losses and then was mounted flatly inside the vacuum chamber of the spectrometer, where the pressure was less than 10^{-5} mbar. The reflectivity of the sample with respect to an Al reference mirror was initially measured. Immediately afterwards, without altering the configuration, gold was evaporated on the sample surface in a built-in evaporator chamber. The reflectivity of the gold-coated surface with respect to the Al mirror was used for correcting the reflectance data by taking into consideration surface imperfections. Hence, the absolute reflectivity of the sample was finally obtained after using the absolute Au values from the literature for the final correction. A variety of light sources, beam splitters, and detectors was used in order to cover the whole frequency range and the overlap between the different regions was excellent.

From the reflectivity data, the optical constants were calculated by Kramers-Kronig (KK) transformation. The Hagen-Rubens relation was used for the low-frequency extrapolation and the power law was used for the high-frequency extrapolation.¹⁴ Values of the optical constants at the limits of the measured region are not expected to be accurate due to the lack of sufficient number of data points that are necessary for the correct calculation of the KK integrals.

III. RESULTS AND DISCUSSION

A. Temperature-dependent conductivity measurements

Temperature-dependent conductivity measurements are widely used as a simple tool for an initial classification of a system in respect to its transport properties.^{4,8,12,15} They can

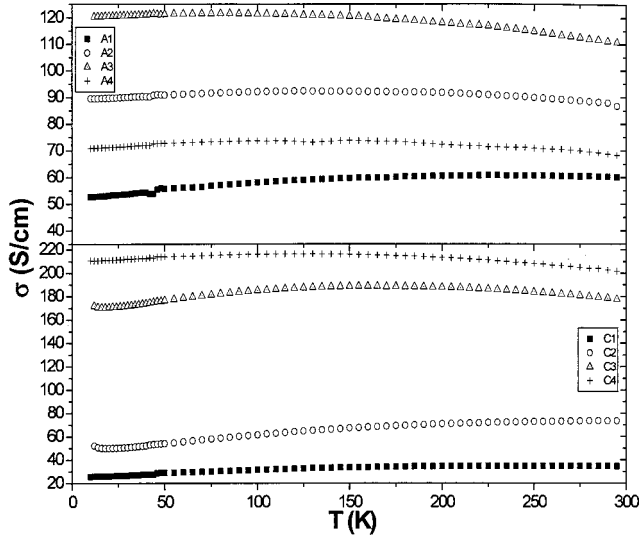


FIG. 2. Temperature dependent dc conductivity graphs for PANi-AMPSA (top) and PANi-CSA (bottom) samples. The positive TCR is more pronounced for the most conducting samples A3 and C4.

provide a qualitative sense of the extent of the disorder present in the sample, since the conductivity is dependent upon the relaxation time, which is controlled by the scattering processes occurring in the material and is, therefore, sensitive to the presence of any disorder in the system. In order to achieve this, the activation energy $W = d(\ln \sigma)/d(\ln T)$, being far more sensitive than the conductivity itself¹⁶ can be used, when the sample shows a weakly negative TCR, at temperatures usually below 40 K. W has a positive temperature coefficient for a sample in the metallic regime, it is temperature independent for a sample in the critical regime and has a negative temperature coefficient for a sample at the insulating side of the I - M transition. In conjunction with the activation energy, a less robust empirical parameter, the resistivity ratio $\rho_r = \sigma(295 \text{ K})/\sigma(10 \text{ K})$ is used for a quick estimate of the sample quality. According to previous studies,^{17,18} for PANi samples in the metallic regime $\rho_r < 2$, while the corresponding limits for critical and insulating behavior are $2 < \rho_r < 5$ and $10 < \rho_r$, respectively.

In order to investigate the effect of the doping on the transport properties of PANi, conductivity measurements on a series of samples were performed and are shown in Fig. 2. The samples were labeled accordingly, and the room-temperature conductivity, the peak conductivity with its respective temperature, and the resistivity ratio are listed in Table I. The values are consistent with previous studies.^{19,20} Despite the fact that measurements at temperatures below 10 K were unattainable inhibiting a more accurate determination of the resistivity ratio, from the low values of ρ_r and the weak temperature dependence of σ demonstrated in Fig. 2, it can be surmised that all the samples are on the metallic side of the I - M transition. The most metallic samples, A3 and C4, have the onset of a positive TCR (i.e., $d\sigma/dT < 0$) at lower temperatures, signifying a decrease in the disorder-induced localization in the system. Samples C2 and C3 seem to have the tendency of a positive TCR at temperatures below 10 K,

TABLE I. The room-temperature conductivity, the peak conductivity with its respective temperature, and the resistivity ratio ρ_r for all the samples examined in Fig. 2.

Sample	σ_{dc} (295 K) (S/cm)	T ($\sigma_{dc}^{\text{peak}}$) (K)	$\sigma_{dc}^{\text{peak}}$ (S/cm)	ρ_r
PANi-AMPSA 30% (A1)	60	230	61	1.140
PANi-AMPSA 40% (A2)	87	125	93	0.969
PANi-AMPSA 50% (A3)	110	80	122	0.920
PANi-AMPSA 60% (A4)	68	150	74	0.963
PANi-CSA 30% (C1)	35	245	35	1.337
PANi-CSA 40% (C2)	73	290	73	1.405
PANi-CSA 50% (C3)	178	160	189	1.034
PANi-CSA 60% (C4)	202	120	216	0.956

however, due to the lack of data points in this region and considering the fact that small fluctuations like those observed are within the experimental error, conclusions about the existence of positive TCR at very low temperatures, like the one observed in ion-implanted PANi,²¹ cannot be made.

Further evidence of the sample's metallic behavior is provided by the activation energy plots W as a function of temperature, as shown in Fig. 3. The positive slope of W is more pronounced for the PANi-CSA samples, whose conductivity shows slightly stronger temperature dependence than the PANi-AMPSA samples. The W plots indicate that the samples are on the metallic side of an I - M transition; some being closer to the critical regime than others according to their doping level. The most conductive samples, A3 and C4, show a rather more erratic behavior in their W plots than the rest of the samples. This can be related to the fact the crossover from negative TCR to positive TCR occurs at considerably lower temperatures, indicating that the electron-phonon scattering increasingly contributes to the transport properties against the interplay of other factors such as disorder, screening, and interactions. The extent of the importance of each of those factors and its contribution to the charge transport is impossible to be assessed from the conductivity data by itself and therefore other measurements, such as magnetoconductance, are necessary for clarifying the situation any further.

B. Infrared reflectivity measurements and optical properties

In order to probe into the subtle differences of the properties exhibited by each PANi sample present in Table I, reflectivity measurements were conducted on the samples that showed the highest and the lowest degree of metallic behavior in each of the two emeraldine salt categories. The room-temperature reflectivity spectra (20 – 9000 cm^{-1}) of films A1 and A3 from the PANi-AMPSA samples, along with C1 and C4 from PANi-CSA, are shown in Fig. 4. All samples manifest reflectivity values greater than 80% in the far infrared ($\omega \leq 100 \text{ cm}^{-1}$), going over 90% for the most conducting samples A3 and C4. The effect of the disorder on the reflectivity values is apparent since the reflectivity drops monotonically until the onset of interband transitions that occur in the visible spectral range.²² Obvious phonon fea-

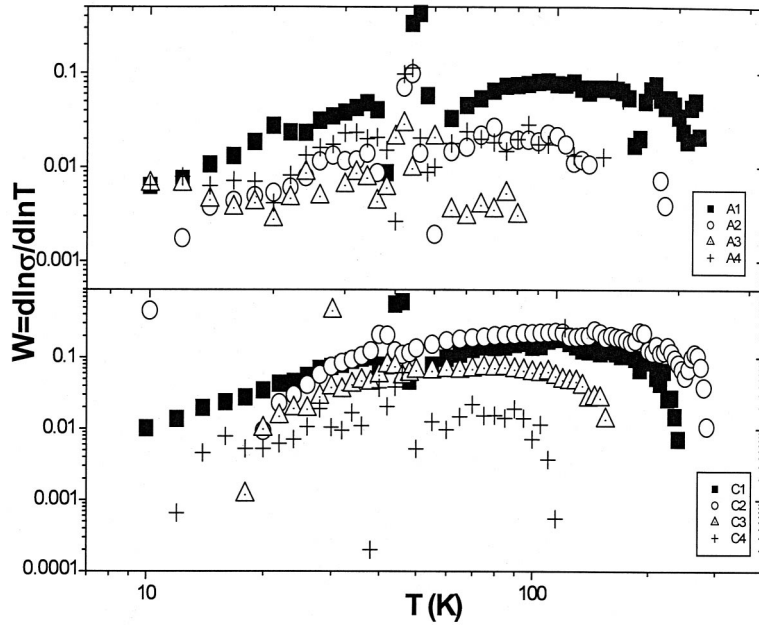


FIG. 3. Log-log plots of the activation energy W against temperature for PANi-AMPSA (top) and PANi-CSA (bottom). Both sets of curves show a prevailing positive slope, even though the PANi-AMPSA curves are considerably more erratic.

tures appear between $200\text{--}2000\text{ cm}^{-1}$ and, contrary to typical metals, are insufficiently screened by the free electrons.

The principal purpose of the reflectivity data is the calculation, through the Kramers-Kronig integral transformations, of the complex dielectric constant, $\epsilon = \epsilon_1 + i\epsilon_2$, which describes the optical properties of the system in more detail. Figure 5 shows the real part of the dielectric function, ϵ_1 , while the imaginary part, ϵ_2 , is plotted in the inset of Fig. 6 along with the energy-loss function $\text{Im}(-1/\epsilon)$. In all the samples, the dielectric function shows after approximately 3500 cm^{-1} , behavior reminiscent of the free electron response in traditional metals at the plasma frequency region. The plasma frequency Ω_p is principally defined as the frequency where $\epsilon_1 = 0$ and $\epsilon_2 \ll 1$, while the energy-loss function, $\text{Im}(-1/\epsilon)$, exhibits a sharp peak.^{23,24} According to the Drude model, the real part of the dielectric function is given by the expression

$$\epsilon_1 = \epsilon_\infty - \frac{\omega_p^2}{\omega^2 + \gamma^2}, \quad (1)$$

where $\omega_p^2 = 4\pi e^2 N/Vm^*$, is the unscreened plasma frequency defined in the Drude Model, N/V is the free carrier concentration, ϵ_∞ is the high-frequency dielectric constant, m^* the effective mass of the charge carriers (which will be considered equal to the free electron mass), and $\gamma = 1/\tau$ is the damping constant which is connected to the relaxation time τ .²⁵ Hence, the relation between the measured plasma frequency Ω_p and ω_p is

$$\Omega_p^2 = \frac{\omega_p^2}{\epsilon_\infty} - \gamma^2. \quad (2)$$

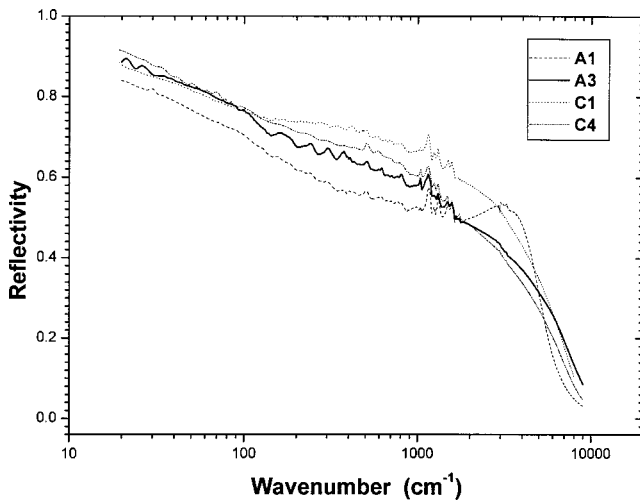


FIG. 4. Semi-log plot of the room-temperature reflectivity for selected PANi samples.

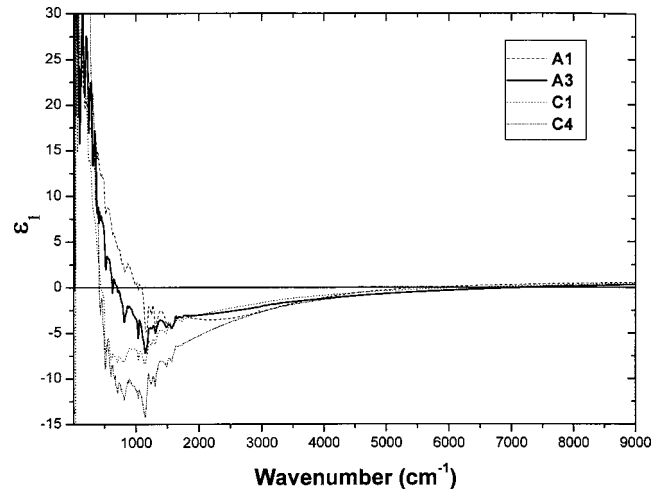


FIG. 5. The real part ϵ_1 of the dielectric function as obtained from a KK transformation of the reflectivity data. All samples display Drude-like behavior after 3500 cm^{-1} with the model curves coinciding with the experimental curves shown here.

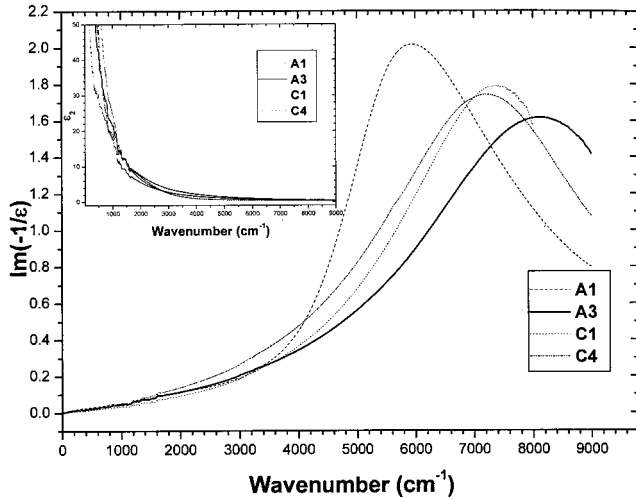


FIG. 6. The energy-loss function $\text{Im}(-1/\epsilon)$ and the imaginary part, ϵ_2 , of the dielectric function (inset). Note that $\text{Im}(-1/\epsilon)$ peaks and $\epsilon_2 \ll 1$ only at the vicinity of the plasma frequency Ω_p .

Equation (1) was fitted to the experimental data curves for frequencies above 3500 cm^{-1} . The fitting procedure generated curves virtually indistinguishable, under the current plot resolution, from the data curves. The fitting parameters ω_p , γ , and ϵ_∞ along with the measured values of Ω_p and $\text{Im}(-1/\epsilon)$ and the free carrier concentration, N/V^{Drude} , are included in Table II.

Although the Drude model describes satisfactorily the free-carrier response at high frequencies, the behavior of the samples below 3000 cm^{-1} does not resemble that of typical metals and therefore cannot be explained by using such a simple model. The localization modified Drude model (LMD) (Refs. 6, 7) is a more suitable candidate for describing the carrier response in the infrared region since it can account for any disorder present in the sample. It is given by

$$\sigma_{\text{LMD}}(\omega) = \sigma_D(\omega) \left\{ 1 - \frac{C}{(k_F \lambda)^2} \left[1 - \left(\frac{3\omega}{\gamma} \right)^{1/2} \right] \right\}, \quad (3)$$

where $\sigma_D(\omega) = \omega_p^2 \gamma / 4\pi(\omega^2 + \gamma^2)$ is the equivalent for optical conductivity of the Drude expression (1), $C \approx 1$, k_F is the Fermi wave vector, and λ the mean free path. Expression (3)

TABLE II. Experimental values of Ω_p and $\text{Im}(-1/\epsilon)$ along with the fitting parameter values ω_p , γ and ϵ_∞ of the Drude model to the experimental data for frequencies above 3500 cm^{-1} and the free carrier concentration N/V^{Drude} . The values for the samples A2 and A4 were taken from Ref. 9.

Sample	Ω_p (cm^{-1})	$\text{Im}(-1/\epsilon)_{\text{peak}}$ (cm^{-1})	ω_p (cm^{-1})	γ (cm^{-1})	ϵ_∞	N/V^{Drude} (10^{20} cm^{-3})
A1	5662	5943	6603	1671	1.2	4.9
A2	7155	7787	9366	4806	1.2	9.8
A3	7230	8190	9201	4354	1.2	9.4
A4	6344	7372	8862	5050	1.2	8.7
C1	6890	7355	8248	3284	1.2	7.6
C4	6332	7173	8477	4387	1.2	8.0

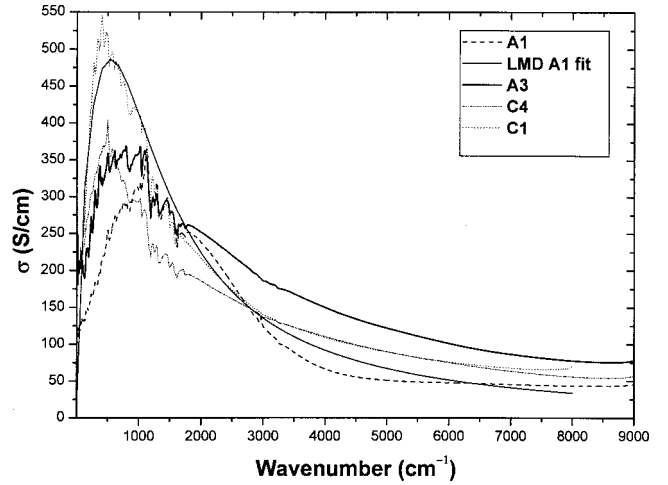


FIG. 7. The real part $\sigma(\omega)$ of the optical conductivity. For clarity purposes, only one of the LMD model curves is shown along with the experimental curves.

was fitted on the experimental curves plotted in Fig. 7 with ω_p , γ , and $k_F \lambda$ as fitting parameters. The fitting results are listed in Table III. Despite the presence of the vibrational features between 200 and 2000 cm^{-1} that are not accounted in the model, the fitting is quite successful since it manages to give consistent values with the dc conductivity (Table I) at the zero frequency limit where it takes the form

$$\sigma_{\text{LMD}}(0) = \frac{\omega_p^2}{4\pi\gamma} \left\{ 1 - \frac{1}{(k_F \lambda)^2} \right\}. \quad (4)$$

This expression cannot be applied for samples with values of $k_F \lambda$ equal to or less than 1, i.e., for samples in the limit of the metal-insulator transition. Attempts have been made^{6,26} to provide a correction in Eq. (4) that accounts for the reduction of energy states due to localization, but not without a considerable ambiguity. However, apart from samples A1 and C1, the values of $\sigma_{\text{LMD}}(0)$, as obtained by Eq. (4), that are listed in Table III are in a very good agreement with the experimental values in Table I which were obtained from direct current measurements. Hence the LMD is suitable for estimating the degree of the disorder present on the sample through the parameter $k_F \lambda$, enabling in this way a characterization of its transport regime. Samples with $k_F \lambda > 1$ are on the metallic side of the metal-insulator transition that occurs when the disorder becomes sufficiently large so that $k_F \lambda$ crosses unity and decreases until $k_F \lambda \ll 1$, where all the states are localized and the material becomes a Fermi glass. A typical value of $k_F \lambda$ for a conventional metal like copper is about 500.

From the values of the unscreened plasma frequency ω_p , as obtained from the LMD model, the free carrier concentration, N/V , can be determined. The free carrier density can then be compared to the effective carrier density, $n_{\text{eff}}(\omega_0)$, that contributes to the optical properties up to frequency $\omega_0 = 8000 \text{ cm}^{-1}$ according to the sum rule,

$$\int_0^{\omega_0} \sigma(\omega) d\omega = \frac{\pi e^2}{2} \frac{n_{\text{eff}}(\omega_0)}{m^*}. \quad (5)$$

TABLE III. The fitting parameters of the LMD model along with the experimental value of plasma frequency Ω_p and other quantities derived from the model such as the screened plasma frequency ω_p , the damping constant γ , the order parameter $k_F\lambda$, the free charge carrier concentration N/V , the effective number of carriers $n_{\text{eff}}(\omega_0)$, the evaluated dc conductivity $\sigma_{\text{LMD}}(0)$, and the percentage of the localized carriers L .

Sample	Ω_p (cm^{-1})	ω_p (cm^{-1})	γ (cm^{-1})	$k_F\lambda$	N/V (10^{20} cm^{-3})	$n_{\text{eff}}(\omega_0)$ (10^{20} cm^{-3})	$\sigma_{\text{LMD}}(0)$ (S/cm)	L (%)
A1	5662	4774	1324	0.92	2.5	4.1		49
A2	7155	6725	2463	1.16	5	5.6	79	49
A3	7230	7033	2311	1.36	5.5	6.0	164	41
A4	6344	6177	2427	1.18	4.3	4.7	74	50
C1	6890	5228	929	0.99	3	5.6		60
C4	6332	6498	2123	1.82	4.7	4.8	217	41

Predictably enough, $n_{\text{eff}}(\omega_0)$ is larger than N/V for all the samples involved, indicating that localized carriers also contribute to optical properties up to 8000 cm^{-1} . These values are significantly smaller than in typical metal ($\sim 10^{22} \text{ cm}^{-3}$), but also considerably larger than in a typical semiconductor ($\sim 10^{15} \text{ cm}^{-3}$), denoting the peculiarity of the conjugated polymers in the realm of electrically conducting materials. The values of free carrier concentration, N/V , obtained from the LMD model are noticeably smaller than the Drude values N/V^{Drude} listed in Table II, suggesting, in accordance with the theory,⁷ that disorder induces the free carrier localization at low frequencies. From the differences in the number of carriers between these two models, the percentage of the localized carriers, L , can be estimated. Since irrespectively of the localization mechanism, there will be a critical energy E_C , the mobility edge, separating localized from extended states,²⁷ L will provide an estimate of the number of carriers close to or below E_C . The results, listed in Table III, show that samples, with similar dc conductivities share the same percentage of carrier localization, contributing, thus, to the general consistency of the applied model.

The above results are consistent with previous studies^{22,28–30} that examine the transport properties of conjugated polymers within the framework of an Anderson-Mott insulator-metal transition due to weak localization. In this context, disorder is considered homogeneous, which implies a localization length greater than the structural coherence length so that the system sees only an average.⁸ Disorder causes localization of the wave functions and while it is below a critical limit, a critical energy E_c (the “mobility edge”) separating localized from nonlocalized states exists. The position of the Fermi level E_F in respect to E_c determines whether the system is on the insulating ($E_F < E_c$ or $k_F\lambda \ll 1$), metallic ($E_F > E_c$ or $k_F\lambda > 1$) side, or at the boundary ($E_F \sim E_c$ or $k_F\lambda \sim 1$) of a disorder driven I - M transition. The recent generation of conducting polymers has given samples with fewer large scale inhomogeneities that dominated the transport properties of previous generations. Hence, the current materials are more highly conducting and homogeneous than before, while the reported localization length (~ 100 – 200 \AA) (Ref. 31) is considerably greater than the structural coherence length ($\sim 20 \text{ \AA}$),³² justifying partly

the application of the homogeneous disorder model for which the Anderson-Mott theory applies.

However, the validity of a model can only be assessed if it can reproduce the experimental data. The above discussion shows a considerable consistency between optical and transport measurements since experimentally measured values of conductivity were reproduced, via Eq. (4), with notable accuracy after the application of the LMD model. The values obtained for the free charge carrier concentration ($\sim 10^{20} \text{ cm}^{-3}$) and the relaxation time ($\tau = 1/\gamma \sim 10^{-15} \text{ sec}$) are characteristic of a dirty metal,³³ implying that the mechanism of transport in conducting polymers, despite their structural difference due to the one-dimensional (1D) polymer chains, is not fundamentally different from the 3D delocalization that takes place in amorphous metallic bundles. Nevertheless, the subtle details of the transport mechanism such as the relative importance of the interplay between the quasi-1D nature of the system and the 3D features due to contribution from interchain and counterion interactions are yet to be decided.

The suitability of the conventional homogeneous disorder model for the understanding of the charge transport mechanism in conducting polymers has been contested in some studies^{27,34–36} and an alternative has been proposed. The inhomogeneous disorder model treats the conducting polymer as a composite system of three-dimensional metallic regions with delocalized charge carriers coupled by disordered quasi-1D amorphous regions of polymer chains where one-dimensional disorder induced localization is dominant.³ The metallic transport occurs when the localization length is larger than the separation between the metallic regions so that charge carriers can percolate through the ordered regions. This model was incited after a zero crossover from positive to negative at the far infrared ($\sim 0.01 \text{ eV}$ or $\sim 80 \text{ cm}^{-1}$) of the real part of the dielectric function of polypyrrole³⁷ and PANi (Ref. 38) was observed. This crossover was attributed to a second plasma frequency due to a small fraction ($\sim 10^{16} \text{ cm}^{-3}$) of delocalized carriers with unusually long scattering time $\tau > 10^{-13} \text{ sec}$. This crossover was observed only for systems on the metallic side of the I - M transition, while for systems on the insulating side $\epsilon_1(\omega)$ remains positive for the entire frequency regime. In the case of the samples studied hereby, a second plasma fre-

quency has not been observed. As Fig. 6 testifies, the values of ϵ_2 remain large enough, while the loss function $\text{Im}(-1/\epsilon)$ does not show any peaks in the far-infrared range, preventing the conditions for the existence of a plasma frequency from being satisfied. The erratic crossovers of ϵ_1 that are observed in the case of samples C4 and A3 at the edge of the measurement range ($<30 \text{ cm}^{-1}$) can therefore be attributed to errors in the KK transformations because of low data point density at the measurement edge (20 cm^{-1}), which the extrapolation procedure cannot fully compensate for. Therefore, it is conjectured that the inhomogeneous disorder model is not suitable for interpreting the materials under investigation.

The importance of doping for the metallic properties of conductive polymers has been unequivocally acknowledged in the field.³⁹ The conductivity of the emeraldine base can increase up to ten orders of magnitude after nonredox doping by a protonic acids, as in the current samples. Although the number of electrons associated with the polymer backbone remains unchanged, the rearrangement of the energy levels after doping affects constructively the charge transport leading to an *I-M* transition at high doping levels. Due to the lack of a widely accepted microscopic charge transport mechanism in doped polymers that would quantitatively estimate the contributions of various factors (such as the electron-phonon interaction, *e-e* interaction, interchain interactions and disorder and their extent, quantum lattice fluctuations, extent of intrachain and interchain delocalization of electronic states, etc.),⁸ it is very difficult to construct a comprehensive model that solely explains the metallic properties as a function of the doping level. However, individual observations can always be useful for establishing a solid basis from which a new approach may flourish. Hence, from the data of Tables I and III, it becomes apparent that the optimum dop-

ing level for the PANi-AMPSA samples is 50%, something that is not unexpected regarding the fact that only two out of four nitrogen sites in a EB repeat unit can be protonated, whereas for PANi-CSA samples is 60%, possible suggesting that doping with CSA is less facile than AMPSA. Samples A1 and C1, i.e., 30% doping level, were found to be at the boundary of the *I-M* transition, while the rest were found at the metallic side, suggesting that high doping concentrations adversely affect the extent of the disorder present at the samples.

IV. CONCLUSION

A comprehensive study regarding the transport and optical properties of a series of polyaniline films has been performed. The films used, had various controlled degrees of doping level in order to investigate the effect of doping level on the electrical properties of the polymer. Temperature-dependent conductivity measurements reveal conductivity values ranging from 35–200 S/cm, while a positive TCR, which characterizes normal metals, is also observed for some samples. The activation energy plots and the resistivity ratio indicate that the samples are close to the boundary of the *I-M* transition. From the infrared reflectivity measurements and their subsequent analysis through the KK transformation, it is surmised that PANi is a disordered metal close to *I-M* transition which is shown to be more suitably interpreted in the context of an Anderson-Mott localization.

ACKNOWLEDGMENTS

This work was supported, in part, by the U.S. Department of Energy, Division of Materials Science, under Contract No. DE-AC02-98CH10886 and by EPSRC (GR/M40387).

¹J. Tsukamoto, *Adv. Phys.* **41**, 509 (1992).

²R. Menon, C. O. Yoon, D. Moses, and A. J. Heeger, in *Handbook of Conducting Polymers*, edited by T. A. Skotheim, R. L. Elsenbaumer, and J. R. Reynolds (Marcel Dekker, New York, 1998).

³R. S. Kohlman and A. J. Epstein, in *Handbook of Conducting Polymers*, edited by T. A. Skotheim, R. L. Elsenbaumer, and J. R. Reynolds (Marcel Dekker, New York, 1998).

⁴R. Kiebooms, R. Menon, and K. Lee, in *Handbook of Advanced Electronic and Photonic Materials and Devices*, edited by H. S. Nalwa (Academic, San Diego, CA, 2001), Vol. 8, p. 10 v.

⁵E. M. Conwell, in *Handbook of Organic Conductive Molecules and Polymers*, edited by H. S. Nalwa (Wiley, New York, 1997), Vol. 4.

⁶N. F. Mott, *Metal-Insulator Transitions* (Taylor & Francis, London, 1990).

⁷N. F. Mott, in *Proceedings of the Thirty First Scottish Universities Summer School in Physics*, edited by D. M. Finlayson (Scottish Universities Summer School in Physics, St. Andrews, 1986).

⁸R. Menon, in *Handbook of Organic Conductive Molecules and Polymers*, edited by H. S. Nalwa (Wiley, Chichester; New York, 1997), Vol. 4, p. 4 v.

⁹G. Tzamalīs, N. A. Zaidi, C. C. Homes, and A. P. Monkman, *J. Phys.: Condens. Matter* **13**, 6297 (2001).

¹⁰P. N. Adams, P. J. Laughlin, A. P. Monkman, and A. M. Kenwright, *Polymer* **37**, 3411 (1996).

¹¹P. N. Adams, P. J. Laughlin, and A. P. Monkman, *Synth. Met.* **76**, 157 (1996).

¹²R. Menon, C. O. Yoon, D. Moses, A. J. Heeger, and Y. Cao, *Phys. Rev. B* **48**, 17 685 (1993).

¹³J. Zhou, G. Tzamalīs, N. A. Zaidi, N. P. Comfort, and A. P. Monkman, *J. Mater. Sci.* **36**, 3089 (2001).

¹⁴D. Y. Smith, in *Handbook of Optical Constants of Solids*, edited by E. D. Palik (Academic, New York, 1998), Vol. I.

¹⁵C. O. Yoon, M. Reghu, D. Moses, and A. J. Heeger, *Phys. Rev. B* **49**, 10 851 (1994).

¹⁶A. Mobius, *Phys. Rev. B* **40**, 4194 (1989).

¹⁷M. Ahlskog, R. Menon, A. J. Heeger, T. Noguchi, and T. Ohnishi, *Phys. Rev. B* **55**, 6777 (1997).

¹⁸M. Ahlskog, M. Reghu, and A. J. Heeger, *J. Phys.: Condens. Matter* **9**, 4145 (1997).

¹⁹E. R. Holland, S. J. Pomfret, P. N. Adams, and A. P. Monkman, *J. Phys.: Condens. Matter* **8**, 2991 (1996).

- ²⁰P. N. Adams, P. Devasagayam, S. J. Pomfret, L. Abell, and A. P. Monkman, *J. Phys.: Condens. Matter* **10**, 8293 (1998).
- ²¹A. N. Aleshin, N. B. Mironkov, A. V. Suvorov, J. A. Conklin, T. M. Su, and R. B. Kaner, *Phys. Rev. B* **54**, 11 638 (1996).
- ²²K. H. Lee, A. J. Heeger, and Y. Cao, *Phys. Rev. B* **48**, 14 884 (1993).
- ²³H. Ehrenreich, in *Proceedings of the International School of Physics "Enrico Fermi," Course XXXIV*, edited by J. Tauc (Academic, Varenna on Lake Como, 1966).
- ²⁴H. Ehrenreich and H. R. Philipp, *Phys. Rev.* **128**, 1622 (1962).
- ²⁵G. Burns, *Solid State Physics* (Academic, New York, 1985).
- ²⁶N. F. Mott and M. Kaveh, *Adv. Phys.* **34**, 329 (1985).
- ²⁷H. C. F. Martens, H. B. Brom, and R. Menon, *Phys. Rev. B* **64**, 201102 (2001).
- ²⁸K. Lee and A. J. Heeger, *Synth. Met.* **84**, 715 (1997).
- ²⁹A. J. Heeger, *J. Supercond.* **14**, 261 (2001).
- ³⁰A. J. Heeger, *J. Phys. Chem. B* **105**, 8475 (2001).
- ³¹M. Reghu, Y. Cao, D. Moses, and A. J. Heeger, *Phys. Rev. B* **47**, 1758 (1993).
- ³²J. P. Pouget, Z. Oblakowski, Y. Nogami, P. A. Albouy, M. Laridjani, E. J. Oh, Y. Min, A. G. Macdiarmid, J. Tsukamoto, T. Ishiguro, and A. J. Epstein, *Synth. Met.* **65**, 131 (1994).
- ³³N. F. Mott and E. A. Davis, *Electronic Processes in Non-Crystalline Materials* (Clarendon, Oxford, 1979).
- ³⁴H. C. F. Martens, J. A. Reedijk, H. B. Brom, D. M. de Leeuw, and R. Menon, *Phys. Rev. B* **63**, 073203 (2001).
- ³⁵J. Joo, S. M. Long, J. P. Pouget, E. J. Oh, A. G. MacDiarmid, and A. J. Epstein, *Phys. Rev. B* **57**, 9567 (1998).
- ³⁶V. N. Prigodin and A. J. Epstein, *Synth. Met.* **125**, 43 (2001).
- ³⁷R. S. Kohlman, Y. Min, A. G. Macdiarmid, and A. J. Epstein, *Synth. Met.* **69**, 211 (1995).
- ³⁸R. S. Kohlman, J. Joo, Y. G. Min, A. G. MacDiarmid, and A. J. Epstein, *Phys. Rev. Lett.* **77**, 2766 (1996).
- ³⁹A. G. MacDiarmid, *Synth. Met.* **125**, 11 (2001).